



J. Serb. Chem. Soc. 87 (0) 1–15 (2022)
JSCS–11912

Journal of
the Serbian
Chemical Society

JSCS@tmf.bg.ac.rs • www.shd.org.rs/JSCS

Original scientific paper
Published 18 November 2022

Influence of N doping on structural and photocatalytic properties of hydrothermally synthesized TiO₂/carbon composites

MARINA M. MALETIĆ^{1*#}, ANA M. KALIJDIS², VLADIMIR LAZOVIĆ³,
SNEŽANA TRIFUNOVIĆ⁴, BILJANA M. BABIĆ³, ALEKSANDRA DAPČEVIĆ^{5#},
JANEZ KOVAC⁶ and MARIJA M. VUKČEVIĆ^{5#}

¹Innovation Center of the Faculty of Technology and Metallurgy, Karnegijeva 4, 11000 Belgrade, Serbia, ²Department of Materials, „Vinča” Institute of Nuclear Sciences – National Institute of the Republic of Serbia, University of Belgrade, Mike Petrovića Alasa 12–14, 11000 Belgrade, Serbia, ³Institute of Physics – National Institute of the Republic of Serbia, University of Belgrade, Pregrevica 118, 11080 Belgrade, Serbia, ⁴Faculty of Chemistry, University of Belgrade, Studentski trg 12–16, 11000 Belgrade, Serbia, ⁵Faculty of Technology and Metallurgy, University of Belgrade, Karnegijeva 4, 11000 Belgrade, Serbia and ⁶Department of Surface Engineering, Institute Jožef Stefan, Jamova cesta 39, 1000 Ljubljana, Slovenia

(Received 8 June, revised 11 October, accepted 15 October 2022)

Abstract: N-doped TiO₂/carbon composites (TiO₂/CN) with different nitrogen content, were obtained starting from titanium isopropoxide and glucose, and by varying the amount of melamine, added to starting reaction mixture. For comparison, an undoped sample (TiO₂/C) was also prepared. Structural and surface characteristics were determined through scanning electron microscopy, thermogravimetric analysis, elemental analysis, Fourier transform infrared spectroscopy, X-ray photoelectron spectroscopy, X-ray diffraction and nitrogen adsorption–desorption isotherms. The photocatalytic activity of TiO₂/CN composites was examined via photocatalytic degradation of methylene blue and multiclass pharmaceuticals from water solution. It was found that N doping of TiO₂/carbon composites induced changes in structural and surface characteristics of TiO₂/CN composites, improving their adsorption, but decreasing photocatalytic efficiency. Nevertheless, TiO₂/CN_{0.05} composite obtained by the hydrothermal synthesis in the presence of glucose and 0.05 g melamine showed the highest efficiency for removing selected pharmaceuticals and methylene blue from aqueous solutions through the combined processes of adsorption in the dark, and photocatalytic degradation under UV and visible irradiation.

* Corresponding author. E-mail: mvukasinovic@tmf.bg.ac.rs

Serbian Chemical Society member.

<https://doi.org/10.2298/JSC220608079M>

Keywords: TiO₂/carbon composites; N-doping; surface properties; photocatalytic properties; pharmaceuticals.

INTRODUCTION

Photocatalysis represents a clean, green and sustainable technology that is constantly being studied and improved for its effective application in removing organic pollutants from the environmental water. Titanium dioxide is one of the most widely used photocatalytic materials in the fields of environmental purification, due to its advantages of good chemical stability, low cost and nontoxicity.¹ However, it is photocatalytically active only under UV light, due to its relatively high band gap energy.² Reduction of the band gap energy, which can be achieved by doping TiO₂ with non-metal elements, such as C, B, S and N,²⁻⁶ spread the spectral response of TiO₂ into the visible region. Also, it was found⁷ that N-doping of TiO₂ enhances the photocatalytic performance under UV irradiation by increasing the specific surface area of a photocatalyst.

To obtain highly reactive photocatalysts, in addition to TiO₂ doping with nitrogen, photocatalysts can be combined with different carbon materials that play the role of catalysts.^{1,8-10} It was found that nitrogen doping combined with some carbon material as a carrier lead to an increase in the specific surface area of the material, as well as its photocatalytic activity under visible irradiation.¹

Previously,⁸ we have used a simple method of hydrothermal synthesis to obtain highly reactive TiO₂/carbon composites for photocatalytic degradation of selected organic pollutants, under UV irradiation. In this work, the hydrothermal method was applied to synthesize the material, photocatalytically active under visible light. N-doped TiO₂/carbon composites (TiO₂/CN), with different nitrogen content, were obtained starting from titanium isopropoxide and glucose, and by varying the amount of melamine, added to starting reaction mixture. Obtained composites were characterized by the means of structural and surface properties. Their photocatalytic activity was tested through the degradation of methylene blue (MB) and selected pharmaceuticals, belonging to classes of antibiotics, painkillers, sedatives and cardiovascular. Additionally, it is important to highlight that some of the examined pharmaceuticals (diclofenac, azithromycin, and erythromycin) were included in the watch list of substances for union-wide monitoring in the field of water policy,¹¹ since their presence may pose a significant risk to the aquatic environment.

EXPERIMENTAL

TiO₂/carbon composites doped with nitrogen (TiO₂/CN) were obtained by hydrothermal synthesis. Starting reaction mixture containing: 37 cm³ glucose solution (30 g dm⁻³), 3 cm³ 35 % hydrochloric acid, 6 cm³ of titanium isopropoxide, and different amounts of melamine (0.05, 0.1 and 0.5 g), was placed in the Teflon lined stainless steel autoclave (50 cm³), and carbonized at a temperature of 160 °C and self-generated pressure for 12 h. The resulting suspension, obtained after the carbonization, was filtered and the precipitate was washed with

distilled water and ethanol and dried at 60 °C overnight. Obtained samples were denoted as TiO₂/CN_{0.05}, TiO₂/CN_{0.1} and TiO₂/CN_{0.5}, respectively, based on the amount of melamine used. For the purpose of comparison, the undoped sample (TiO₂/C) was prepared according to the same procedure, without melamine adding.

Scanning electron microscopy (Mira Tescan 3X, Tescan Orsay Holding, Czech Republic) was used to examine the structure and morphology of prepared carbon composites.

The thermogravimetric analysis (TGA, SDT Q600, TA Instruments) was performed in the O₂ atmosphere (flow rate: 100 cm³ min⁻¹) from room temperature up to 800 °C, with a heating rate of 20 °C min⁻¹.

Elemental analysis (Vario EL III Element Analyzer, Elementar, Shimadzu Europe) was performed to determine the nitrogen content in the synthesized composite materials.

Fourier transform infrared spectroscopy (FTIR, Bomem MB-Series, Hartmann Braun) was used for qualitative analysis of surface functional groups. FTIR spectra were obtained in the wavenumber range from 400 to 4000 cm⁻¹.

X-Ray photoelectron spectroscopy (XPS) measurements were performed on the PHI-TFA XPS spectrometer produced by Physical Electronics Inc. and equipped with the monochromatic X-ray source with the Al anode. Wide energy range XPS spectra were taken with pass energy of 187 eV to identify present elements and high-energy resolution XPS spectra were taken with pass energy 29 eV to identify chemical bonds of elements on the surface. Low-energy electron gun was used for neutralization of possible charging effects.

The specific surface area and the pore size distribution (PSD) of carbon composites were analyzed using the Surfer (Thermo Fisher Scientific, USA). PSD was estimated by applying Barrett–Joyner–Halenda (BJH) method¹² to the desorption branch of isotherms and mesopore surface (S_{meso}) and micropore volume (V_{micro}) were estimated using the *t*-plot method.¹³

X-ray diffraction (XRD) patterns were performed by Philips PW1710 diffractometer with CuK α radiation at a scanning speed 1 °C min⁻¹ in the range of 2θ of 20–60°. Based on obtained X-ray diffraction patterns, crystalline phases have been identified, and approximate share of the individual phases in the product and the crystallite size was calculated by computer program Powder Cell.¹⁴

The photocatalytic activity of TiO₂/CN composites, as well as undoped TiO₂/C composite, was evaluated by photocatalytic degradation of methylene blue (MB) and selected pharmaceuticals from multicomponent solution. Experiments were carried out at room temperature and atmospheric pressure with constant shaking on a magnetic stirrer. The starting concentration of the MB solution was 25 mg dm⁻³, while the concentration of composite material was 2 g dm⁻³. The suspension was held for 60 min in the dark until an adsorption–desorption equilibrium is reached, after which the suspension was exposed to UV irradiation. Process of photocatalytic degradation was monitored by periodic sampling (60, 75, 90, 105, 120, 150 and 180 min), and measuring of MB concentration. To compare the photocatalytic activity of examined samples under visible irradiation, MB solution with an initial concentration of 10 mg dm⁻³ was used. As a source of UV irradiation, 125 W high-pressure mercury lamp, Philips, HPLN was used, while visible irradiation was obtained by 150 W tungsten halogen lamp with a 400 nm cut off glass optical filter.

Also, TiO₂/CN composites were used as photocatalysts for degradation of the selected pharmaceuticals: diclofenac (painkillers); bromazepam (sedatives); atorvastatin, amlodipine, cilazapril and clopidogrel (cardiovascular); azithromycin, doxycycline and erythromycin (antibiotics). The initial concentration of each of the selected pharmaceuticals from the multicomponent solution was 5 mg dm⁻³. The concentration of composite photocatalysts was 1 g

dm^{-3} , while experimental conditions were the same as for degradation of MB under UV irradiation. The solution samples were taken after 180 min of the removal process, which included 60 min of adsorption in the dark, followed by photocatalytic degradation. Samples were filtered through $0.45 \mu\text{m}$ PVDF syringe filters, and the concentration of selected pharmaceuticals was assessed by high-performance liquid chromatography–tandem mass spectrometry (LC–MS/MS Thermo Scientific). LC–MS/MS method conditions are given in the Supplementary material to this paper.

RESULTS AND DISCUSSION

The morphological characteristics of TiO_2/CN samples were examined by scanning electron microscopy (Fig. 1). Compared to the undoped sample (Fig. 1d), the addition of melamine in the reaction mixture does not lead to any important differences in the morphology of obtained composites. SEM photographs showed that all N-doped $\text{TiO}_2/\text{carbon}$ composites were characterized by a similar and homogenous structure, regardless of the amount of melamine added to the reaction mixture.

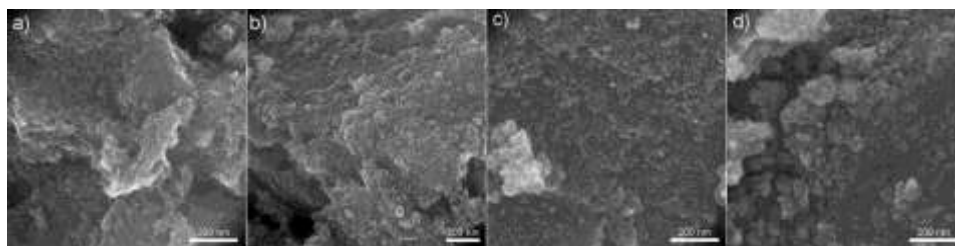


Fig. 1. SEM photographs of samples: a) $\text{TiO}_2/\text{CN}_{0.5}$; b) $\text{TiO}_2/\text{CN}_{0.1}$, c) $\text{TiO}_2/\text{CN}_{0.05}$ and d) TiO_2/C .

The contents of nitrogen, carbon phase and TiO_2 in examined composites were obtained by elemental and thermogravimetric analysis. The TGA, DTG, and DTA curves of the TiO_2/CN composites, as well as undoped TiO_2/C , are shown in Fig. 2a–c, respectively. For all examined samples, according to the DTG curves, the first mass loss was observed in the temperature range from 40 to $120 \text{ }^\circ\text{C}$, which originates from physically and chemically adsorbed water. The second mass loss observed in the range 250 – $450 \text{ }^\circ\text{C}$, is a consequence of hydrothermal carbon oxidation during TG analysis. Sample $\text{TiO}_2/\text{CN}_{0.05}$ has an additional mass loss in the temperature range 550 – $650 \text{ }^\circ\text{C}$, which origin is not fully understood.

According to the literature¹⁵ the mass loss in this region can be the consequence of the decomposition of residual melamine, which is unlikely because samples obtained with a higher amount of melamine do not display the mass loss in this temperature region. Also, it is suggested that the mass loss in the temperature region from 350 – $800 \text{ }^\circ\text{C}$ can be a result of carbon residue degradation, as well as TiO_2 crystal phase transformation.¹⁶ The content of TiO_2 , carbon

phase (obtained from TGA), and nitrogen (from elemental analysis) in examined composites are presented in Table I. Percentage contents of TiO₂ and carbon phase, shown in Table I, were calculated taking the content of hydrothermally obtained TiO₂ on 800 °C as 100 %.

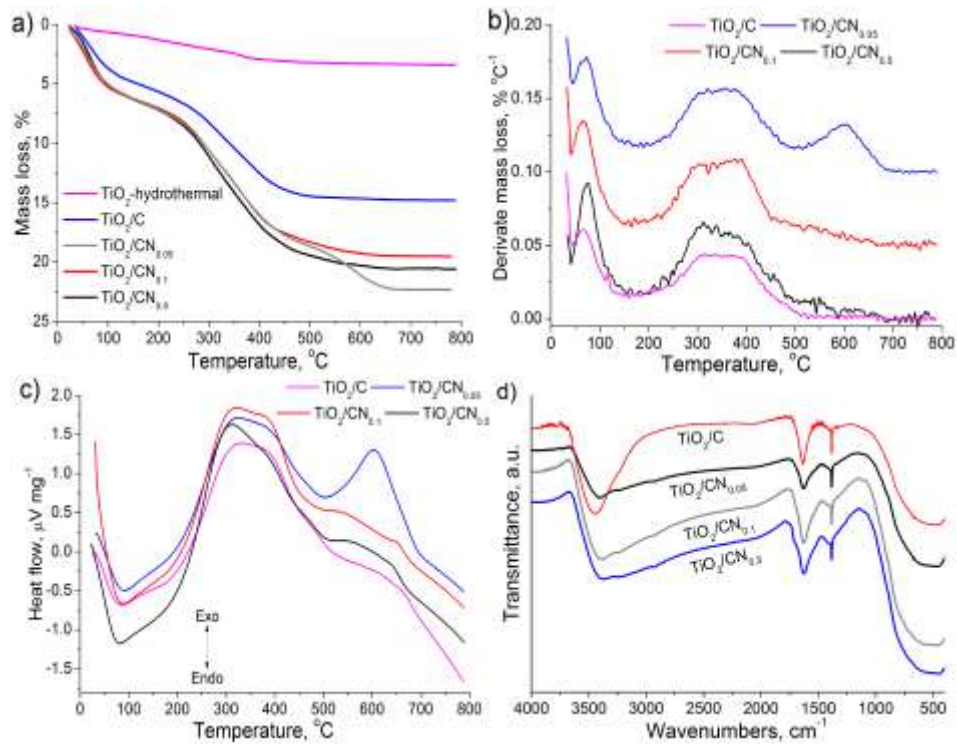


Fig. 2. TGA (a), DTG (b) and DTA (c) curves, and FTIR spectra (d) of TiO₂/C and TiO₂/CN composites.

Table I. TiO₂, carbon phase and nitrogen content in TiO₂/CN composites (wt. %)

Sample	Component		
	TiO ₂	Carbon phase	N
TiO ₂ /C	88.17	11.83	0
TiO ₂ /CN _{0.05}	80.45	19.33	0.221
TiO ₂ /CN _{0.1}	83.27	16.61	0.156
TiO ₂ /CN _{0.5}	82.23	17.48	0.292

Obtained results showed that adding the melamine to the reaction mixture led to nitrogen incorporation into TiO₂/CN composites in the range from 0.156 to 0.292 wt. %. However, nitrogen content in TiO₂/CN composites is not directly dependent on the amount of melamine added to the reaction mixture since both, the lowest and the highest amount of melamine, led to similar nitrogen content in

the TiO₂/CN composites. It has been observed that the lowest concentration of melamine in the reaction mixture resulted in increased content of the organic carbonaceous phase at the expense of the TiO₂ inorganic phase.

FTIR spectra of undoped and doped composites are shown in Fig. 2d. The broad band in the range of 400–1000 cm⁻¹ is derived from the stretch vibration of Ti–O and Ti–O–Ti bonds.^{17,18} The peak at 3400 cm⁻¹ originates from the stretching vibration of the OH bond in Ti–OH and in water adsorbed on the TiO₂ surface, indicating the presence of hydroxyl groups on the surface of the material.¹⁸ Another peak that may correspond to bending vibrations of the O–H bond in water molecules appears around 1625 cm⁻¹ for all tested samples.¹⁸ Two weak peaks at 2850 and 2920 cm⁻¹ can be ascribed to characteristic stretching vibrations of aliphatic C–H, which indicate the formation of carbon layers.¹⁷ The addition of melamine leads to a broadening of the peak at 3400 cm⁻¹. It is necessary to highlight that there are no distinct differences between the FTIR spectra of TiO₂/CN composites. Nevertheless, a small shoulder at around 1715 cm⁻¹, was observed for sample TiO₂/CN_{0.5}. This peak may originate from stretching vibration of –C=O from carbonyl and carboxyl groups, indicating that N-doping with the highest amount of melamine induced their formation. Although the peak at 1385 cm⁻¹ can be related to C=C and O–H bond,¹⁹ it may also be induced by the C–N bond. However, this observation could not confirm the presence of nitrogen in obtained composite materials, since undoped TiO₂/C spectra displayed peaks at the same wavenumber.

XPS analysis was conducted to confirm the nitrogen incorporation into TiO₂/CN composites and to identify the valence state of the doping nitrogen. Fig. 3a shows the very similar spectra of undoped TiO₂/C and TiO₂/CN samples, doped with various nitrogen amounts, taken in the binding energy range from 0 to 1200 eV. In the high-resolution spectra of Ti 2p (Fig. 3b), peaks at 458.8 and 464.4 eV correspond to Ti 2p_{3/2} and Ti 2p_{1/2}, respectively.²⁰ Binding energy difference between these two peaks is 5.6 eV. Binding energy 458.8 eV of Ti 2p_{3/2} confirms the presence of the Ti⁴⁺ states in TiO₂. Fig. 3c shows the high resolution XPS spectra of O 1s, deconvoluted in three peaks at 530.1, 531.7 and 532.8 eV that are ascribed to lattice oxygen (Ti–O–Ti), surface hydroxyl groups (Ti–O–H) and adsorbed water.^{21,22}

The C 1s spectrum (Fig. 3d) was fitted with four peaks. The main peak at 284.8 eV corresponds to C–C and C–H bonds,²³ while the peak at 289.6 eV corresponds to O=C–O. Peaks at 286.4 and 288.4 eV can be assigned to nitrogen-doped sp² carbon (C–N) and nitrogen-doped sp³ carbon (C=N),²⁰ although, these peaks may be related to the C–O, C–OH and C=O, due to much higher concentration of oxygen, compared to nitrogen. Furthermore, the high-resolution N 1s spectra display a peak of around 400 eV (Fig. 3e). Emission in the 399–400 eV region can originate from nitriles (N triple-bonded to only one carbon), graphitic

N (bonded to three carbons),²⁴ or adsorbed nitrogen, but also from the interstitial integration of nitrogen into TiO₂ lattice.

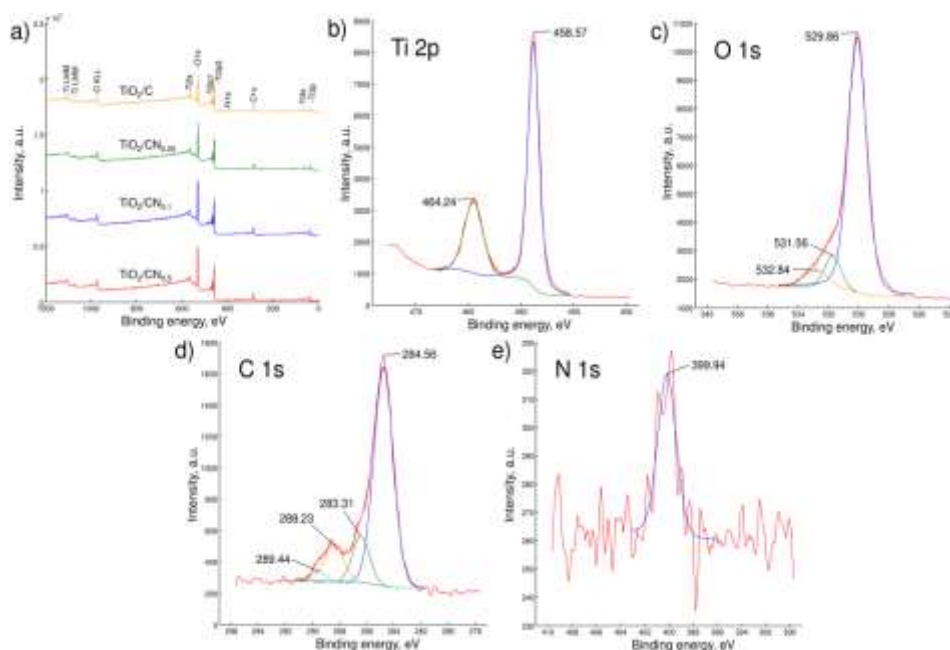


Fig. 3. XPS survey spectra of TiO₂/C and TiO₂/CN samples with various nitrogen content (a), the high-resolution spectra of Ti 2p (b), O 1s (c), C 1s (d) and N 1s (e) of TiO₂/CN_{0.5}.

Nitrogen adsorption isotherms obtained for undoped and TiO₂/CN samples are given in Fig. 4a, as the dependence of the adsorbed amount of N₂ ($n / \text{mmol g}^{-1}$) and relative pressure (P/P_0) at the temperature of liquid nitrogen. Obtained isotherms are type IV of IUPAC classification,²⁵ containing a hysteresis loop, which indicates a mesoporous material. The observed hysteresis loop of type H2 is typical for the pores of undefinable shape.

Additionally, non-limiting adsorption at high P/P_0 , observed for N-doped samples indicates the presence of slit-shaped pores at non-rigid aggregates of plate-like particles.²⁶ Pore size distribution (Fig. 4b) for all samples is very narrow and close to the limiting value between micro and mesopores (2 nm). This means that these materials can be considered microporous with a small fraction of mesoporousness. Values for the average pore width (r_D), for all samples, along with the calculated porosity parameters (S_{BET} , S_{meso} , S_{mic} , V_{mic}) are given in Table II. The mesoporous TiO₂/C sample showed an S_{BET} of 174.08 m² g⁻¹ and an average pore width of 3.78 nm.

On the other hand, all TiO₂/CN composites are mainly microporous, with a maximum pore radius of about 2.2 nm. Also, it was found that the S_{BET} of

N-doped samples, ranging from 186 to 239 $\text{m}^2 \text{g}^{-1}$, increase with nitrogen content. Consideration of the obtained results indicates that melamine addition in reaction mixture leads to the decrease of average pore width, and drastically increases the microporosity, as well as S_{BET} values of obtained TiO_2/CN samples. As it was reported previously,²⁷ these changes in specific surface area and average pore width may be the consequence of the substitution of carbon atoms, most likely located on the reactive edges, with nitrogen atoms during hydrothermal synthesis. These incorporated N atoms could act as a catalyst for porosity development.

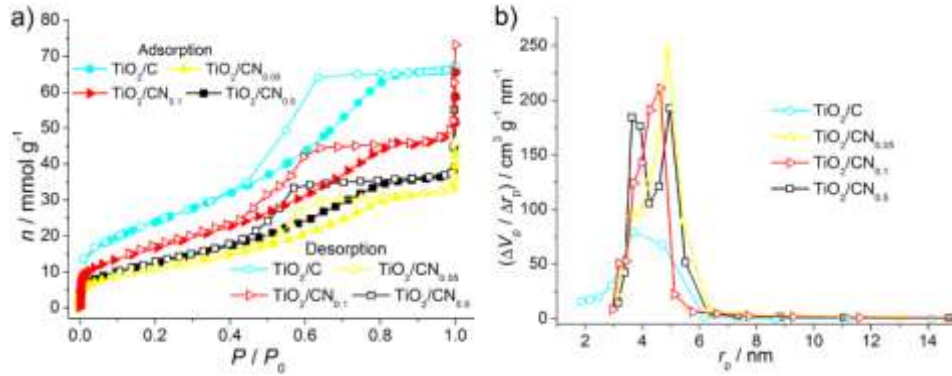


Fig. 4. Nitrogen adsorption isotherms (a) and pore size distribution (b) for TiO_2/C and TiO_2/CN samples.

TABLE II. Porous properties of TiO_2/CN samples

Sample	$S_{\text{BET}} / \text{m}^2 \text{g}^{-1}$	$S_{\text{meso}} / \text{m}^2 \text{g}^{-1}$	$S_{\text{mic}} / \text{m}^2 \text{g}^{-1}$	$V_{\text{mic}} / \text{cm}^3 \text{g}^{-1}$	r_p / nm
TiO_2/C	174	168	6	0.048	3.78
$\text{TiO}_2/\text{CN}_{0.05}$	231	32	199	0.231	2.37
$\text{TiO}_2/\text{CN}_{0.1}$	186	17	169	0.194	2.11
$\text{TiO}_2/\text{CN}_{0.5}$	239	22	217	0.246	2.38

XRD analysis was performed to determine the content of crystalline TiO_2 phases in TiO_2/C and TiO_2/CN composites, as well as the crystallite size. XRD diffraction pattern for all tested samples (Fig. 5) showed the presence of a characteristic peak for anatase (101) ($2\theta = 25.6^\circ$) crystalline phase, as well as peaks at 2θ 38.2 (112), 48.3 (200) and 54.6° (105) also arising from anatase crystalline modification.^{10,28} The presence of a low-intensity peak at $2\theta = 27.7^\circ$ (110), originating from rutile crystal modification, was observed for the undoped sample TiO_2/C (Fig. 5).²⁸ However, no distinguish peaks characteristic for the rutile phase were displayed on XRD diffraction patterns of TiO_2/CN composites. A shoulder appearing at $2\theta = 26^\circ$ (110), visible on the XRD diffraction pattern of all TiO_2/CN composites, may originate from the photocatalytically inactive crys-

talline phase of brookite, as well as from titanium nitride.²⁹ The presence of these phases may affect the photocatalytic activity of the examined composites, especially of sample TiO₂/CN_{0.5} which shows the shoulder of higher intensity. Although XPS analysis showed that nitrogen was most likely incorporated in carbon lattice, the addition of melamine to the starting reaction mixture affected the structure of N-doped composites by favoring the formation of the anatase phase and suppressing the formation of the rutile phase.

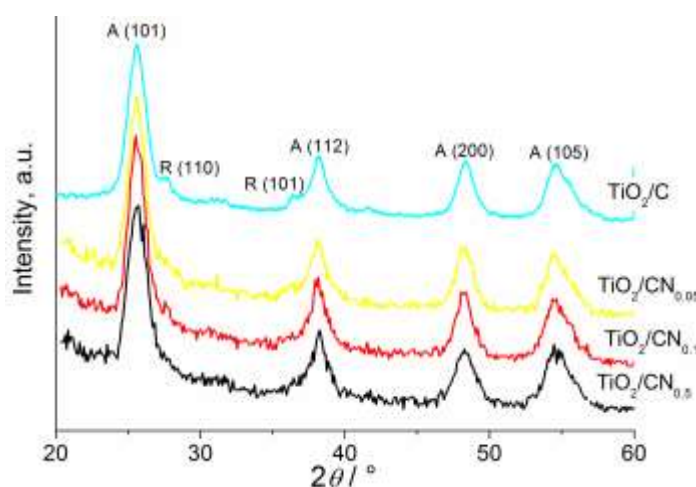


Fig. 5. XRD patterns of examined samples.

The calculated approximate values of the fraction of TiO₂ crystalline phases and the size of the crystallite are shown in Table III. The undoped sample, TiO₂/C, contains 24 % of the rutile phase, while N doping significantly decreased the content of the rutile phase. The observed increase of the anatase phase content should favorably affect the photocatalytic characteristics of TiO₂/CN composites. It can be noticed that N-doping leads to a decrease in the average grain size, which is dependable on nitrogen content in TiO₂/CN composites. The addition of melamine increases the content of amorphous carbon (Table I), which inhibits the growth of TiO₂ grains and thus N-doping leads to a decrease in the grain size. Obtained values for grain size and average pore width (Table II), suggest that these pores most likely represent interparticle spaces.

The photocatalytic activity of TiO₂/CN composites was investigated in the process of removing methylene blue from aqueous solutions under UV and visible irradiation. Fig. 6a shows the photocatalytic decomposition of MB as a decrease in the MB concentration during the time. The entire process of MB removal lasted 180 min and it was performed in two steps. The first step is related to the establishment of an adsorption/desorption equilibrium for 60 min in the dark, and the second step implied the degradation of organic pollutants in the

presence of UV or visible irradiation. Fig. 6b summarized the removal efficiency after the first adsorption step in the dark, the second step of photocatalytic degradation under UV irradiation, and total removal efficiency. At the end of the first step, TiO₂/CN samples showed higher adsorption capacity (removing 44–70 % of MB) than sample TiO₂/C, which adsorbed about 35 % of the initial amount of MB. According to the results shown in Fig. 6b and Table II, adsorption efficiency increases with specific surface area, although, a direct relationship between S_{BET} and the amount of MB adsorbed cannot be established. N-doped samples had higher adsorption capacity, but lower photocatalytic efficiency since N-doped samples showed lower removal efficiency during the irradiation step than the undoped sample. However, according to Fig. 6b, samples TiO₂/CN_{0.5} and TiO₂/CN_{0.05} showed the highest level of adsorption and total removal efficiency, due to the high specific surface area, which is the result of the highest content of carbon. Photocatalytic characteristics of examined materials are not directly influenced by nitrogen content. TiO₂/C showed better photocatalytic activity than N-doped samples, most likely because increased carbon content in N-doped samples had a negative effect on photocatalytic activity by preventing light penetration to the TiO₂.

TABLE III. Anatase and rutile phase content and grain sizes of TiO₂/C and TiO₂/CN composites

Sample	Crystallite size, nm	Phase content, wt. %	
		Anatase	Rutile
TiO ₂ /C	9.76	76.0	24.0
TiO ₂ /CN _{0.05}	7.15	98.0	2.0
TiO ₂ /CN _{0.1}	7.26	99.0	1.0
TiO ₂ /CN _{0.5}	6.52	95.0	5.0

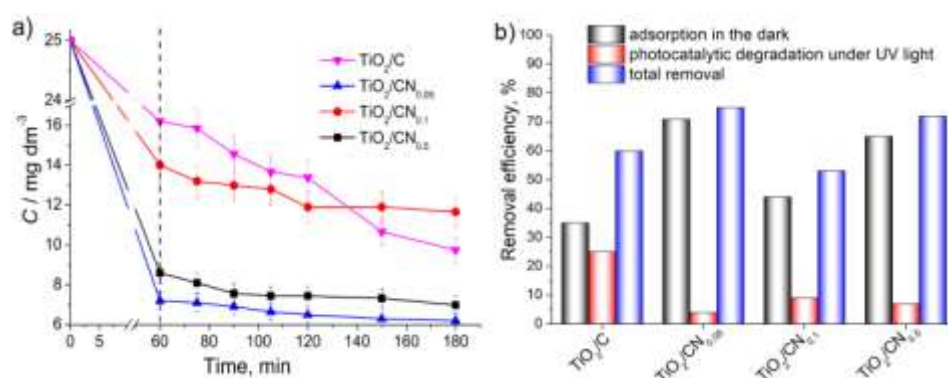


Fig. 6. Photocatalytic decomposition (a) and removal efficiency (b) of MB in the presence of TiO₂/C and TiO₂/CN composites.

Undoped and N-doped samples showed a similar trend in the photocatalytic activity in the process of methylene blue removal under visible irradiation (Fig. 7a). Samples obtained by adding a larger amount of melamine to the reaction mixture (TiO₂/CN_{0.1}, TiO₂/CN_{0.5}) show lower photocatalytic activity in the visible region than the undoped sample. Only the sample obtained with a small amount of melamine (TiO₂/CN_{0.05}) shows a better efficiency than the undoped sample. As was already mentioned, due to the large specific surface area and the highest carbon content, sample TiO₂/CN_{0.05} displayed the best efficiency in the MB removal process. Also, its photocatalytic activity in the decomposition of MB under visible radiation ($\lambda > 400$ nm) was followed by the recording of the absorption spectra. According to the spectra shown (Fig. 7b), no new absorption bands appear in the visible or UV area, which confirms the disappearance of the dye chromophore structure.³⁰ Even though the absorption peak at 663 nm decreases with the increase in reaction time, the MB is not degraded after 24 h.

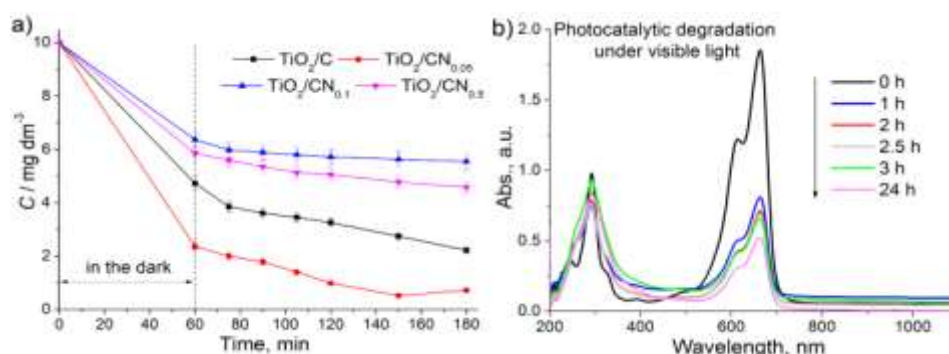


Fig. 7. Photocatalytic decomposition of MB in the presence of undoped and N-doped samples (a) and absorption spectra of MB on TiO₂/CN_{0.05} (b).

The possibility of removing selected pharmaceuticals from a multi-component solution by TiO₂/CN composites under UV irradiation was also examined. For the purpose of comparison, results obtained by undoped TiO₂/C composite were also presented. Fig. 8 summarized the percentage of removed pharmaceuticals by adsorption in the dark, followed by the photocatalytic degradation under UV irradiation after 180 min, and total removal efficiency.

Generally, all tested materials better adsorb pharmaceuticals of decreased polarity (higher values of retention time in Table S-II of the Supplementary material), except in the case of doxycycline. The higher specific surface area of N-doped samples, compared to the undoped sample, positively affects the pharmaceutical adsorption, except for amlodipine adsorption where the undoped sample showed the highest removal efficiency in the dark. Samples TiO₂/CN_{0.1} and TiO₂/CN_{0.5} show a lower efficiency of pharmaceuticals removal under UV

irradiation (Fig. 8b), compared to the undoped sample and $\text{TiO}_2/\text{CN}_{0.05}$. Nevertheless, all tested composites demonstrate high efficacy in the total removal (Fig. 8c) of diclofenac, doxycycline, atorvastatin, amlodipine and clopidogrel, which were completely removed after the adsorption in the dark, followed by photocatalytic degradation under UV irradiation.

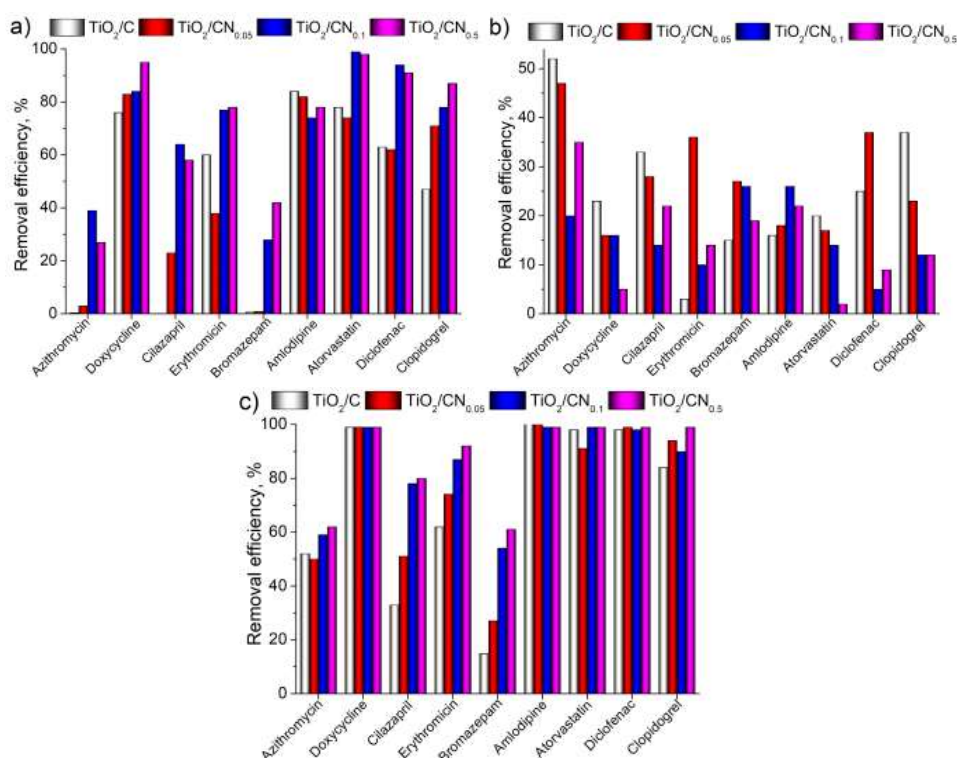


Fig. 8. Removal of pharmaceuticals from a multi-component solution by TiO_2/C and TiO_2/CN composites: a) adsorption in the dark, b) under UV irradiation and c) total removal.

The percentage of totally removed pharmaceuticals increases with the higher amount of melamine introduced in the starting reaction mixture, most likely due to the increased specific surface area and adsorption efficiency. In that way, the composite obtained with the highest amount of melamine, $\text{TiO}_2/\text{CN}_{0.5}$, showed the highest efficiency for removing selected pharmaceuticals from aqueous solutions.

CONCLUSION

N-doped $\text{TiO}_2/\text{carbon}$ composites were obtained by hydrothermal synthesis using melamine, as a source of nitrogen, though the nitrogen content in TiO_2/CN composites was not directly proportional to the amount of melamine added to the

reaction mixture. The incorporation of nitrogen affected the structural and surface characteristics of composite photocatalysts, by increasing the specific surface area and microporosity, as well as the content of the photocatalytically active anatase phase. N-doping affected the efficiency of these composites to remove methylene blue and selected pharmaceuticals, by increasing their adsorption efficiency and decreasing photocatalytic activity under UV irradiation. Nevertheless, TiO₂/CN_{0.05} composite, obtained by the hydrothermal synthesis in the presence of glucose and 0.05 g melamine, showed the highest efficiency for removing selected pharmaceuticals and methylene blue from aqueous solutions through the combined processes of adsorption in the dark and photocatalytic degradation under UV and visible irradiation.

SUPPLEMENTARY MATERIAL

Additional data and information are available electronically at the pages of journal website: <https://www.shd-pub.org.rs/index.php/JSCS/article/view/11912>, or from the corresponding author on request.

Acknowledgements. The research was funded by the Ministry of Education, Science and Technological Development of the Republic of Serbia (Contract Nos. 451-03-68/2022-14/200135, 451-03-68/2022-14/200287 and 451-03-9/2021-14/200017).

ИЗВОД

УТИЦАЈ ДОПИРАЊА АЗОТОМ НА СТРУКТУРНЕ И ФОТОКАТАЛИТИЧКЕ КАРАКТЕРИСТИКЕ ХИДРОТЕРМАЛНО СИНТЕТИСАНИХ TiO₂/КАРБОН КОМПЗИТА

МАРИНА М. МАЛЕТИЋ¹, АНА М. КАЛИЈАДИС², ВЛАДИМИР ЛАЗОВИЋ³, СНЕЖАНА ТРИФУНОВИЋ⁴,
БИЉАНА М. БАБИЋ³, АЛЕКСАНДРА ДАПЧЕВИЋ⁵, JANEZ KOVAČ⁶ и МАРИЈА М. ВУКЧЕВИЋ⁵

¹Иновациони Центар Технолошко–металуршког факултета, Карнегијева 4, 11000 Београд,
²Лабораторија за материјале, Институт за нуклеарне науке Винча – Институт од националне значаја, Универзитет у Београду, Мике Пешировића Аласа 12–14, 11000 Београд, ³Институт за физику – Институт од националне значаја, Универзитет у Београду, Предревца 118, 11080 Београд, ⁴Хемијски факултет, Универзитет у Београду, Студентски тир 12–16, 11000 Београд, ⁵Технолошко–металуршког факултета, Универзитет у Београду, Карнегијева 4, 11000 Београд и ⁶Department of Surface Engineering, Institute Jožef Stefan, Jamova cesta 39, 1000 Ljubljana, Slovenia

TiO₂/карбон композити допирани азотом (TiO₂/CN) добијени су хидротермалном карбонизацијом смеше титан изопропоксида и глукозе, у присуству различитих количина меламина као прекурсора азота. Извршена је површинска и структурна карактеризација материјала, а добијени резултати су упоређени са карактеристикама недопираниог TiO₂/карбон композита. Фотокаталитичка активност добијених композита испитана је фотокаталитичком разградњом метиленско плавог и лекова из мултикомпонентног воденог раствора. Утврђено је да допирање азотом TiO₂ карбон композита доводи до промена у структурним и површинским карактеристикама TiO₂/CN композита, побољшавајући њихову адсорпциону ефикасност, али смањујући фотокаталитичку активност. Показано је да се примењеном методом хидротермалне карбонизације могу добити ефикасни композити за уклањање одабраних лекова и метиленског плавог из водених раствора, применом процеса адсорпције у мраку, праћеног фотокаталитичком разградњом под UV и видљивим зрачењем.

(Примљено 8. јуна, ревидирано 11. октобра, прихваћено 15. октобра 2022)

REFERENCES

1. N. C. T. Martins, J. Ângelo, A.V. Girão, T. Trindade, L. Andrade, A. Mendes, *Appl. Catal., B* **193** (2016) 67 (<http://dx.doi.org/10.1016/j.apcatb.2016.04.016>)
2. B. Farkas, P. Heszler, J. Budai, A. Oszkó, M. Ottosson, Z. Geretovszky, *Appl. Surf. Sci.* **433** (2018) 149 (<https://doi.org/10.1016/j.apsusc.2017.09.181>)
3. R. Asahi, T. Morikawa, H. Irie, T. Ohwaki, *Chem. Rev.* **114** (2014) 9824 (<https://dx.doi.org/10.1021/cr5000738>)
4. Y.T. Lin, C.H. Weng, Y.H. Lin, C.C. Shiesh, F.Y. Chen, *Sep. Purif. Technol.* **116** (2013) 114 (<http://dx.doi.org/10.1016/j.seppur.2013.05.018>)
5. K. Siuzdak, M. Szkoda, A. Lisowska-Oleksiak, K. Grochowska, J. Karczewski, J. Ryl, *Appl. Surf. Sci.* **357** (2015) 942 (<http://dx.doi.org/10.1016/j.apsusc.2015.09.130>)
6. K. Pathakoti, S. Morrow, C. Han, M. Pelaez, X. He, D. D. Dionysiou, H. M. Hwang, *Environ. Sci. Technol.* **47** (2013) 9988 (<https://dx.doi.org/10.1021/es401010g>)
7. N. X. Qian, X. Zhang, M. Wang, X. Sun, X. Y. Sun, C. Liu, R. Rao, Y. Q. Ma, *J. Photochem. Photobiol., A* **386** (2020) 112127 (<https://doi.org/10.1016/j.jphotochem.2019.112127>)
8. M. Maletić, M. Vukčević, A. Kalijadis, I. Janković-Častvan, A. Dapčević, Z. Laušević, M. Laušević, *Arab. J. Chem.* **12** (2019) 4388 (<http://dx.doi.org/10.1016/j.arabjc.2016.06.020>)
9. M. Maletić, M. Vukčević, A. Kalijadis, Z. Laušević, M. Laušević, *Adv. Mater. Sci. Eng.* (2015) 803492 (<http://dx.doi.org/10.1155/2015/803492>)
10. H. Belayachi, B. Bestani, N. Benderdouche, M. Belhakem, *Arab. J. Chem.* **12** (2019) 3018 (<http://dx.doi.org/10.1016/j.arabjc.2015.06.040>)
11. Commission implementing Decision (EU) 2015/495, *Off. J. Eur. Union* **L78(58)** (2015) 40 (<https://eur-lex.europa.eu/legal-content/EN/TXT/?uri=uriserv%3AOJ.L.2015.078.01.0040.01.ENG&toc=OJ%3AL%3A2015%3A078%3ATOC>)
12. E.P. Barrett, L.G. Joyner, P.P. Halenda, *J. Am. Chem. Soc.* **73** (1951) 373 (<https://doi.org/10.1021/ja01145a126>)
13. B.C. Lippens, B.G. Linsen, J.H. De Boer, *J. Catal.* **3** (1964) 32 ([https://doi.org/10.1016/0021-9517\(64\)90089-2](https://doi.org/10.1016/0021-9517(64)90089-2))
14. W. Kraus, G. Nolze, *Powder Cell for Windows*, V.2.4, Federal Institute for Materials Research and Testing, Berlin (<https://powdercell-for-windows.software.informer.com/2.4/>)
15. M. Sathish, B. Viswanathan, R. P. Viswanath, *Appl. Catal., B* **74** (2007) 307 (<https://doi.org/10.1016/j.apcatb.2007.03.003>)
16. J. Zhang, Y. Li, L. Li, W. Li, C. Yang, *ACS Sustain. Chem. Eng.* **6** (2018) 12893 (<https://doi.org/10.1021/acssuschemeng.8b02264>)
17. H. He, H. Wang, D. Sun, M. Shao, X. Huang, Y. Tang, *Electrochim. Acta* **236** (2017) 43 (<http://dx.doi.org/10.1016/j.electacta.2017.03.104>)
18. K. Kalantari, M. Kalbasia, M. Sohrabi, S. J. Royae, *Ceram. Int.* **43** (2017) 973 (<http://dx.doi.org/10.1016/j.ceramint.2016.10.028>)
19. H. Safardoust-Hojaghan, M. Salavati-Niasari, *J. Clean. Prod.* **148** (2017) 31 (<http://dx.doi.org/10.1016/j.jclepro.2017.01.169>)
20. W. Ji, Y.G. Mei, M. Yang, H. Liu, S. Wang, Z. Shan, F. Ding, X. Liu, X. Gao, X. Li, *J. Alloys Compd.* **806** (2019) 946 (<https://doi.org/10.1016/j.jallcom.2019.07.225>)
21. Y. Li, H. Li, X. Lu, X. Yu, M. Kong, X. Duan, G. Qin, Y. Zhao, Z. Wang, D. D. Dionysiou, *J. Colloid Interface Sci.* **596** (2021) 384 (<https://doi.org/10.1016/j.jcis.2021.03.140>)

22. X. Chen, D. H. Kuo, D. Lu, *Chem. Eng. J.* **295** (2016) 192 (<http://dx.doi.org/10.1016/j.cej.2016.03.047>)
23. A. Kalijadis, J. Đorđević, T. Trtić-Petrović, M. Vukčević, M. Popović, V. Maksimović, Z. Rakočević, Z. Laušević, *Carbon* **95** (2015) 42 (<http://dx.doi.org/10.1016/j.carbon.2015.08.016>)
24. N. Hellgren, R.T. Haasch, S. Schmidt, L. Hultman, I. Petrov, *Carbon* **108** (2016) 242 (<http://dx.doi.org/10.1016/j.carbon.2016.07.017>)
25. K.S.W. Sing, D.H. Everett, R.A.W. Haul, L. Moscou, R.A. Pierotti, J. Rouquerol, T. Siemieniowska, *Pure Appl. Chem.* **57** (1985) 603 (<https://doi.org/10.1351/pac198557040603>)
26. S. Lowell, J.E. Shields, M.A. Thomas, M. Thommes, *Characterization of Porous Solids and Powders: Surface Area, Pore Size and Density*, Kluwer Academic Publishers, Dordrecht, 2004 (<https://doi.org/10.1007/978-1-4020-2303-3>)
27. A. Kalijadis, N. Gavrilov, B. Jokić, M. Gilić, A. Krstić, I. Pašti, B. Babić, *Mater. Chem. Phys.* **239** (2020) 122120 (<https://doi.org/10.1016/j.matchemphys.2019.122120>)
28. E. Kordouli, K. Bourikas, A. Lycourghiotis, C. Kordulis, *Catal. Today* **252** (2015) 128 (<http://dx.doi.org/10.1016/j.cattod.2014.09.010>)
29. A.D. Paola, M. Bellardita, L. Palmisano, *Catalysts* **3** (2013) 36 (<http://doi:10.3390/catal3010036>)
30. G. Dai, S. Liu, Y. Liang, H. Liu, Z. Zhong, *J. Mol. Catal., A* **368–369** (2013) 38 (<http://dx.doi.org/10.1016/j.molcata.2012.11.014>).

